Steady-State Performance Analysis of an Integrated Wind Turbine Generating System in a DC Transmission System with Power Compensation System

Ken-ichiro Yamashita *, Shoji Nishikata **

Abstract – An electric power compensation system for a DC transmission system with an integrated wind turbine generator is proposed. The proposed compensation system consists of a synchronous generator and a duplex reactor. This apparatus is connected to the sending-end circuit of the DC transmission system. A set of steady-state equations of the system is first derived. Then, the effect of the duplex reactor, which can eliminate the sending-end grid current distortion due to commutation of the converter, is explored. The relationships among power at the sending-end circuit are also revealed. It is shown that fluctuations in the sending-end grid power due to changes in wind velocities are compensated with the proposed system. Finally, the effects of the sending-end grid conditions on the steady-state characteristics of the system are studied.

Keywords: DC power transmission, Power control, Power conversion, Thyristor circuits, Wind power generation

1. Introduction

The utilization of renewable energy sources such as wind power is one of the most useful ways to maintain the environment. In large-scale wind farms, the interconnecting method of wind turbine generators with grids is a major issue. We have studied a wind turbine generating system using a shaft generator system [1]-[4], which is widely used for power sources in large ships [5], and have proposed a DC transmission system with an integrated wind turbine generating system as one of the interconnecting methods [6]. The proposed DC transmission system has high reliability and a smoothing capacitor is not required since a current-source thyristor inverter and converters are adopted. Moreover, this system requires only one inverter to operate many wind turbine generators simultaneously. Furthermore, it can generate high quality electrical power without distortion [3]. These features of the system are advantages for large-scale wind farms.

In [7], we have investigated the steady-state characteristics of the proposed DC transmission system and have explored compensating methods for fluctuations in the receiving-end grid power due to changes in wind velocities. However, compensating methods for the sending-end grid power have been little discussed. In this paper, a sending-end grid power compensation system for the DC transmission system including wind turbine generators is proposed.

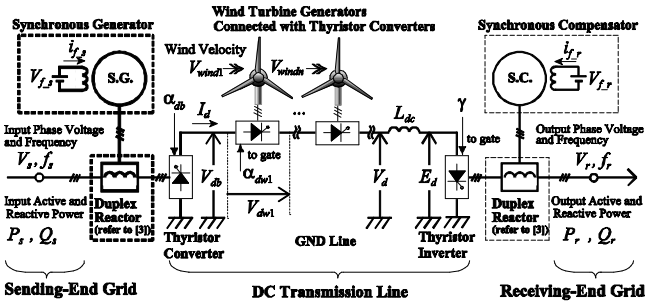

Fig. 1. Configuration of the proposed DC transmission system including wind turbine generating systems

A configuration of the proposed DC transmission system with the power compensating system is shown in Fig. 1. In this system, AC power produced by the wind turbine generator is converted into DC power with the thyristor converter, and this DC power is combined with the power of the DC transmission system. The total DC power is converted into AC power with the thyristor inverter. In addition, the synchronous compensator connected to the receiving-end grid provides reactive power for the grid and for commutation of the inverter thyristors. Then, receiving-end grid output voltage harmonics can be eliminated with the duplex reactor [3]. The power compensating system proposed in this paper consists of a synchronous generator

* Dept. of Electrical Engineering, Salesian Polytechnic, Tokyo, Japan. (yamasita@salesio-sp.ac.jp)
** Dept. of Electrical and Electronic Engineering, Tokyo Denki University, Tokyo, Japan. (west@cck.dendai.ac.jp)
Received 05 July 2011 ; Accepted 19 October 2011

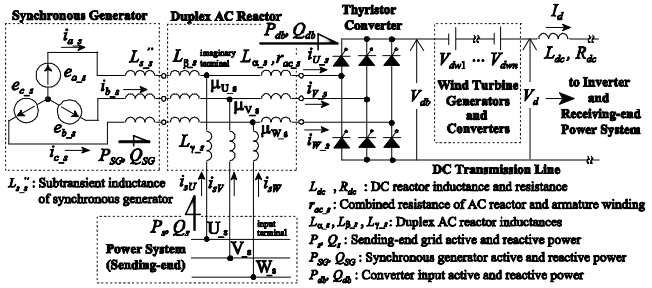

Fig. 2. Equivalent circuit of the sending-end circuit for the proposed system

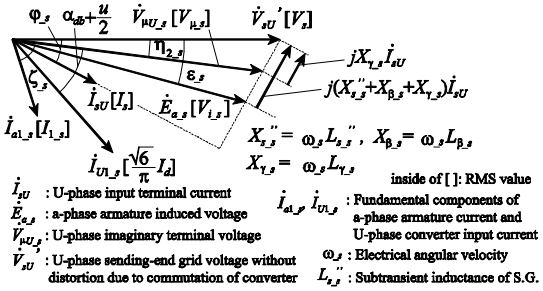

Fig. 3. Phasor diagram (per phase)

and a duplex reactor. This apparatus is connected to the sending-end grid to compensate fluctuations in the sending-end grid power and to eliminate harmonic components of the sending-end grid current. As in Fig. 1, since the sending-end circuit is the same as the receiving-end circuit, the power flow of the whole system can be easily controlled.

In this paper, the steady-state equations of the proposed system are derived first. Then, the effect of the sending-end duplex reactor is explored, and the steady-state characteristics of the power at the sending-end circuit are revealed. Finally, the effects of the sending-end grid conditions on the steady-state characteristics of the system are investigated and the appropriate conditions of the sending-end grid are discussed.

2. Derivation of Steady-State Equations

In Fig. 2, the equivalent circuit is shown to derive the steady-state equations of the sending-end circuit for the proposed system with the power compensating system. In this figure, several sets of wind turbine generating systems are represented as DC voltage sources V_{dw1}, V_{dw2}, . . . , V_{dwn} respectively. It is also assumed that the sending-end grid current distortion is eliminated completely with the duplex reactor. Fig. 3 shows the phasor diagram of the fundamental components of the voltages and currents in the sending-end circuit given in Fig. 2 (per phase).

Let us now derive the steady-state equations of the sending-end circuit. In [5] – [7], a set of equations of the system without the power compensating system proposed here have already been derived, and these equations can be applicable.

Based on Figs. 2 and 3, the RMS value of the imaginary terminal μ_s phase voltage V_{μ_s} and the lagging angle η_{2_s} are obtained by:

$$V_{\mu\_s} = \sqrt{\left(V_s - X_{\gamma\_s} I_s \sin\varphi_{\_s}\right)^2 + \left(X_{\gamma\_s} I_s \cos\varphi_{\_s}\right)^2} \quad (1)$$

$$\eta_{2\_s} = \tan^{-1}\left\{\left(X_{\gamma\_s} I_s \cos\varphi_{\_s}\right)/\left(V_s - X_{\gamma\_s} I_s \sin\varphi_{\_s}\right)\right\} \quad (2)$$

where, V_s: sending-end input terminal phase voltage, I_s: input terminal current at the sending-end, $\varphi_{\_s}$: power factor angle of the sending-end grid, X_{γ_s}: sending-end circuit duplex reactor reactance.

The armature induced voltage of the synchronous generator can be assumed to be sinusoidal when it has damper windings. The RMS value of the armature induced voltage V_{i_s} and the lagging angle $\varepsilon_{\_s}$ are given by:

$$V_{i\_s} = \sqrt{\left(V_s - \left(X_{\beta\_s} + X_{\gamma\_s} + X_{s\_s}"\right) I_s \sin\varphi_{\_s}\right)^2 + \left(\left(X_{\beta\_s} + X_{\gamma\_s} + X_{s\_s}"\right) I_s \cos\varphi_{\_s}\right)^2} \quad (3)$$

$$\varepsilon_{\_s} = \tan^{-1} \frac{\left(X_{\beta\_s} + X_{\gamma\_s} + X_{s\_s}"\right) I_s \cos\varphi_{\_s}}{V_s - \left(X_{\beta\_s} + X_{\gamma\_s} + X_{s\_s}"\right) I_s \sin\varphi_{\_s}} \quad (4)$$

where, X_{β_s}: sending-end circuit duplex reactor reactance, $X_{s\_s}"$: subtransient reactance of the synchronous generator.

The angle of overlap of converter input currents u_s is expressed as follows:

$$u_{\_s} = -\alpha_{db} + \cos^{-1}\left\{\cos\alpha_{db} - \frac{2\left(X_{s\_s}" + X_{\alpha\_s} + X_{\beta\_s}\right) I_d}{\sqrt{6} V_{\mu\_s}}\right\} \quad (5)$$

where, α_{db}: firing angle of the sending-end converter, X_{α_s}: sending-end duplex reactor reactance, I_d: DC link current.

The RMS value of the fundamental component of the armature current I_{1_s} and the lagging angle $\zeta_{\_s}$ can be given by:

$$I_{1\_s} = \sqrt{\left(\sqrt{6} I_d / \pi\right)^2 + I_s^{\,2} - 2\left(\sqrt{6} I_d / \pi\right) I_s \times \cos\left(\eta_{2\_s} + \alpha_{db} + u_{\_s}/2 - \varphi_{\_s}\right)} \quad (6)$$

$$\zeta_{\_s} = \varphi_{\_s} - \varepsilon_{\_s} + \sin^{-1}\left\{\frac{\sqrt{6} I_d}{\pi I_{1\_s}} \sin\left(\eta_{2\_s} + \alpha_{db} + \frac{u_{\_s}}{2} - \varphi_{\_s}\right)\right\} \quad (7)$$

On the other hand, the DC side voltage for the sending-end circuit V_{db} shown in Fig. 2 is expressed as:

$$V_{db} = \frac{3\sqrt{6}}{\pi} V_{\mu\_s} \cos\alpha_{db} - E_{x\_s} \tag{8}$$

$$E_{x\_s} = \frac{3}{\pi}\left(X_{\alpha\_s} + X_{\beta\_s} + X_{s\_s}''\right) I_d \tag{9}$$

$$E_{x\_s} = \frac{3\sqrt{6}}{2\pi} V_{\mu\_s}\left(\cos\alpha_{db} - \cos\overline{\alpha_{db} + u_{\_s}}\right) \tag{10}$$

Similarly, the average value of the inverter DC side voltage E_d can be obtained by [5]:

$$E_d = \frac{3\sqrt{6}}{\pi} V_{\mu\_r} \cos\gamma + E_{x\_r} \tag{11}$$

$$E_{x\_r} = \frac{3}{\pi}\left(X_{\alpha\_r} + X_{\beta\_r} + X_{s\_r}''\right) I_d \tag{12}$$

$$E_{x\_r} = \frac{3\sqrt{6}}{2\pi} V_{\mu\_r}\left(\cos\overline{\gamma - u_{\_r}} - \cos\gamma\right) \tag{13}$$

where, V_{μ_r}: receiving-end circuit imaginary terminal phase voltage, X_{α_r}, X_{β_r}: receiving-end circuit duplex reactor reactances, X_{s_r}'': subtransient reactance of the synchronous compensator shown in Fig. 1, $u_{\_r}$: overlap angle of inverter currents, γ: leading angle of commutation of the inverter.

Moreover, the DC side voltage of the ith (i = 1, 2, . . . , n) wind turbine generator to obtain the maximum power from the wind turbine V_{dwopi} is expressed as follows [7], [8]:

$$V_{dwopi} = \left\{P_{tmaxi} - R_{\omega i} \cdot (\lambda_{opi} / R_{ri})^2 \cdot V_{windi}{}^2\right\} / I_d \tag{14}$$

$$P_{tmaxi} = 0.5 \cdot C_{pmaxi} \cdot \rho \cdot A_i \cdot V_{windi}{}^3 \tag{15}$$

where, P_{tmaxi}: the maximum output power derived from the ith wind turbine, $R_{\omega i}$: damping coefficient, λ_{opi}: the optimum tip speed ratio, R_{ri}: blade radius, V_{windi}: wind speed, C_{pmaxi}: the maximum power coefficient, ρ: the air density, A_i: rotor swept area. When the maximum power is obtained, the ith wind turbine generator DC side voltage V_{dwi} is equal to V_{dwopi}.

From (8), (11), and (14), the total DC side voltage V_d can be expressed as [7]:

$$V_d = V_{db} + V_{dw1} + \cdots + V_{dwn} = RI_d + E_d \tag{16}$$

where, $R = R_{dc} + 2r_{ac\_s} + 2r_{ac\_r}$, R_{dc}: DC reactor resistance, r_{ac_s}, r_{ac_r}: combined resistances of the AC reactor and the armature winding of the synchronous machine at the sending-end and receiving-end circuits respectively.

Fig. 4 shows the equivalent circuit of the synchronous generator to derive steady-state equations considering magnetic saturation. In the following, the steady-state

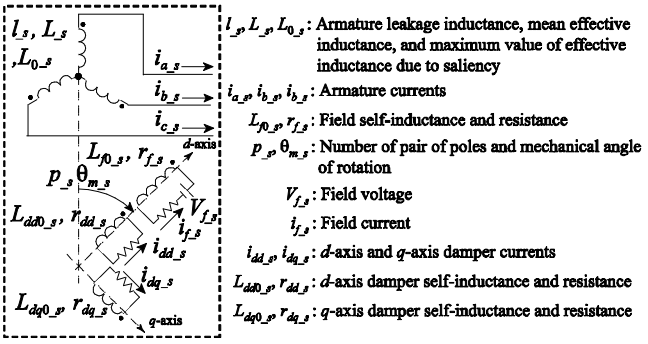

Fig. 4. Equivalent circuit of the synchronous generator

equations for the synchronous generator are derived based on Fig. 4 and [4].

The voltage equation of the field winding is expressed as:

$$V_{f\_s} = r_{f\_s} \cdot i_{f\_s} \tag{17}$$

where, V_{f_s}: field voltage, r_{f_s}: field resistance, i_{f_s}: field current.

The air-gap flux linkage of the synchronous generator ψ_{g_s} can be obtained by:

$$\psi_{g\_s} = \sqrt{\left(k_{d\_s}\psi_{dd\_s}\right)^2 + \left(k_{q\_s}\psi_{q0\_s}\right)^2} \tag{18}$$

$$k_{d\_s} = L_{add\_s} / L_{dd0\_s} \tag{19}$$

$$k_{q\_s} = L_{adq\_s} / L_{dq0\_s} \tag{20}$$

where, L_{add_s}, L_{adq_s}: maximum value of mutual inductances between armature winding and d-axis damper winding, q-axis damper winding, respectively, L_{dd0_s}, L_{dq0_s}: d-axis and q-axis damper self-inductances, ψ_{dd_s}, ψ_{q0_s}: total magnetic flux linkages of the d-axis and q-axis damper windings and these are given by:

$$\psi_{dd\_s} = 3\sqrt{2}/2 \cdot I_{1\_s} \cdot L_{add\_s} \sin\left(-\alpha_{\_s} - \zeta_{\_s}\right) + L_{fdd\_s} \cdot i_{f\_s} \tag{21}$$

$$\psi_{q0\_s} = -3\sqrt{2}/2 \cdot I_{1\_s} \cdot L_{adq\_s} \cos\left(-\alpha_{\_s} - \zeta_{\_s}\right) \tag{22}$$

$$\alpha_{\_s} = \tan^{-1}\left\{-k_{q\_s}\psi_{q0\_s} / \left(k_{d\_s}\psi_{dd\_s}\right)\right\} \tag{23}$$

where, L_{fdd_s}: mutual inductance between field winding and d-axis damper winding, $\alpha_{\_s}$: shift angle due to armature reaction.

Based on [4], the steady-state equations considering magnetic saturation of the synchronous generator are given by:

$$\overline{X_{ds\_s}} = \overline{X_{ds0\_s}}/2\left\{\left(1-\overline{k_{1\_s}}\cdot\overline{\psi_{g\_s}}\right)\right.$$
$$\left.+\sqrt{\left(1-\overline{k_{1\_s}}\cdot\overline{\psi_{g\_s}}\right)^2-\overline{k_{2\_s}}\cdot\overline{\psi_{g\_s}}^2}\right\} \quad (24)$$

$$\overline{X_{ad\_s}} = \overline{X_{ds\_s}} - \overline{X_{l\_s}} \quad (25)$$

$$\overline{X_{aq\_s}} = k_{a\_s}\overline{X_{ad\_s}} \quad (26)$$

$$\overline{X_{s\_s}}'' = \sigma_{d\_s}\overline{X_{ds\_s}} \quad (27)$$

where, $\overline{X_{ds\_s}}$: *d*-axis synchronous reactance, $\overline{X_{ds0\_s}}$, $\overline{k_{1\_s}}$, $\overline{k_{2\_s}}$, k_{a_s}, σ_{d_s}: the parameters of considering magnetic saturation of the synchronous generator refer to [4], $\overline{X_{ad\_s}}$, $\overline{X_{aq\_s}}$: *d*-axis and *q*-axis armature reaction reactances, $\overline{X_{l\_s}}$: armature leakage reactance. In (24) – (27), '–' show per-unit representation. The base values in the per-unit system are given in [9].

On the other hand, the steady-state equations of the power at the sending-end circuit can be expressed by [7], [10]:

$$P_{db} = 3\sqrt{6}/(2\pi)V_{\mu\_s}\left(\cos\alpha_{db}+\cos\overline{\alpha_{db}+u_{\_s}}\right)I_d \quad (28)$$

$$Q_{db} = I_d\sqrt{\left(3\sqrt{6}/\pi\cdot V_{\mu\_s}\right)^2 - V_{db}^2} \quad (29)$$

$$P_{SG} = P_{db} - P_s = P_{db} - 3V_sI_s\cos\varphi_{\_s} \quad (30)$$

$$Q_{SG} = Q_{db} - Q_s = Q_{db} - 3V_sI_s\sin\varphi_{\_s} \quad (31)$$

By using these equations and the equations derived in [6] and [7], we can examine the steady-state performances of the proposed DC transmission system.

3. Steady-State Characteristics

Let us discuss the steady-state characteristics of the system through the theory and experiments for a tested system when one wind turbine generator is connected to the DC transmission system. The ratings of the synchronous generator of the tested system are 2.77(kVA), 4poles, 200(V), and 8(A). Then, the constants needed to calculate the steady-state characteristics are shown in Table 1. In addition, the sending-end grid and receiving-end grid are assumed to be infinity bus.

3.1 Effect of the sending-end duplex reactor

The receiving-end duplex reactor can eliminate the receiving-end grid output voltage distortion [3]. Here, let us discuss the effect of the sending-end duplex reactor. The.

Table 1. Parameters of the Tested System and Simulated Wind Turbine (per-unit representation)

Synchronous machine				DC transmission system	
X_{ad_s}	0.429 pu	X_{ds0_s}	0.429 pu	R	0.149 pu
X_{aq_s}	0.208 pu	X_{dq0_s}	0.208 pu		
r_{f_s}	0.003484 pu	X_{s_s}''	0.123 pu	AC Reactor	
k_{a_s}	0.485	X_{ds0_s}	0.824 pu	X_{α_s}	0.184 pu
σ_{d_s}	0.212	k_{1_s}	0.143 pu	X_{β_s}	-0.123 pu
X_{l_s}	0.15 pu	k_{2_s}	0.393 pu	X_{γ_s}	0.368 pu
Wind turbine (rating of turbine power is 0.1pu)					
C_{pmaxi}	0.436	ρ	1.0 pu	R_{r_i}	9.028 pu
λ_{opi}	5.52	$R_{\omega i}$	0 pu	A_i	0.459 pu

Notes – the parameters of the receiving-end are the same values of the parameters shown in this table. When wind velocity is 10m/s, which is the rated wind speed, the output power of the simulated wind turbine is 277W. All wind turbines connected to the system have the same parameters shown in this table.

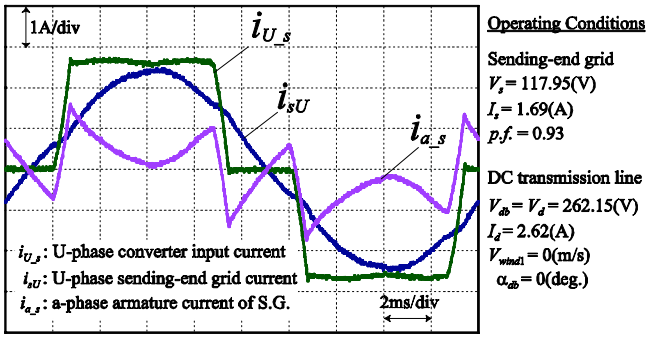

Fig. 5. Measured sending-end circuit current waveforms

sending-end grid current distortion due to commutation of the converter thyristors will be eliminated because the subtransient inductance of the synchronous generator is canceled out by the sending-end circuit duplex reactor

Fig. 5 shows current waveforms of the converter input terminal, the synchronous generator output terminal, and the input terminal at the sending-end for the tested system. The conditions for the waveforms are given in the figure. From this figure, it is shown that, although there were harmonics in the converter input current and in the synchronous generator output current waveforms due to the commutation of the converter thyristors, almost no distortion in the sending-end grid current waveform was obtained, supporting the usefulness of the sending-end duplex reactor.

3.2 Steady-state characteristics of the sending-end circuit

In the DC transmission system without a power compensating system, fluctuations in the power at the receiving-end grid due to changes in wind velocities can be

compensated by the input DC power control and the sending-end grid power is varied with the changes in the input DC power [7]. In the case with the proposed power compensating system, the synchronous generator is connected to the sending-end circuit and provides active and reactive power for the sending-end circuit to suppress the fluctuations in the power at the sending-end grid.

Fig. 6 shows the steady-state characteristics of the synchronous generator output active and reactive power P_{SG}, Q_{SG}, the sending-end converter input active and reactive power P_{db}, Q_{db}, the sending-end grid active and reactive power P_s, Q_s, the DC side voltages at the sending-end circuit and the wind turbine generating system V_{db}, V_{dw1}, and the field current of the synchronous generator i_{f_s} when the wind velocity V_{wind1} was changed. The system conditions are given in Fig. 6(a). From Fig. 6, it is shown that the measured and calculated results are in good agreement, supporting the theory derived in this paper. It is clarified from Fig. 6(c) that V_{dw1} is increased with V_{wind1} because V_{dw1} is controlled in order to obtain the maximum DC input power from the wind turbine generating system. In this case, V_{db} is reduced with the increase in V_{wind1} to maintain the total DC side voltage V_d constant. It can be seen that, although the reduction in V_{db} causes the decrease in P_{db}, a constant power at the sending-end grid P_s can be obtained by controlling P_{SG} for the case with the power compensating system. It is also shown that, although the converter input reactive power Q_{db} is increased as shown in Fig. 6(b) due to the increase in α_{db} required for the decrease in V_{db}, the sending-end grid reactive power Q_s can be kept constant. This is because the synchronous generator can operate as a synchronous compensator to supply sufficient reactive power (Q_{SG}). In this case, the field current i_{f_s} is increased as shown in Fig. 6(c).

3.3 Effects of the sending-end grid conditions on the steady-state characteristics of the system

In the foregoing discussions, it has been confirmed that the constant sending-end grid power and the sending-end grid current without distortion can be obtained for the case with the proposed electrical power compensation system. We discuss here the effects of the sending-end grid conditions on the steady-state characteristics of the system.

In Fig. 7, the characteristics of the sending-end imaginary terminal μ_s phase voltage V_{μ_s}, the sending-end circuit DC side voltage V_{db}, the sending-end converter input active and reactive power P_{db}, Q_{db} versus the sending-end grid active power P_s for three values of the sending-end grid power factor are shown. The system conditions needed to calculate the characteristics are expressed in Fig. 7(a). It

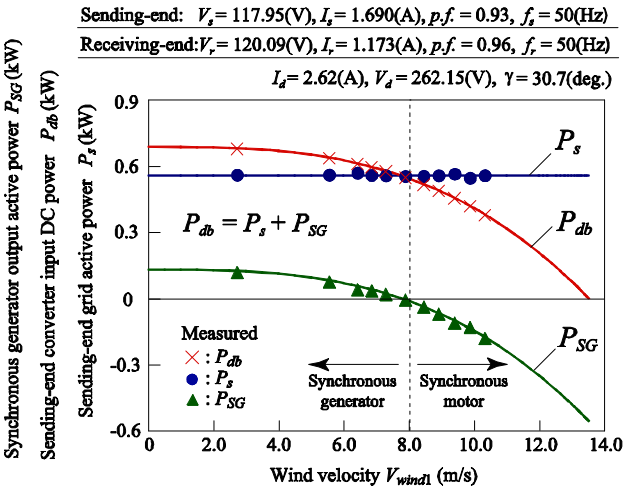

(a) Active power of the sending-end circuit P_{SG}, P_{db}, P_s

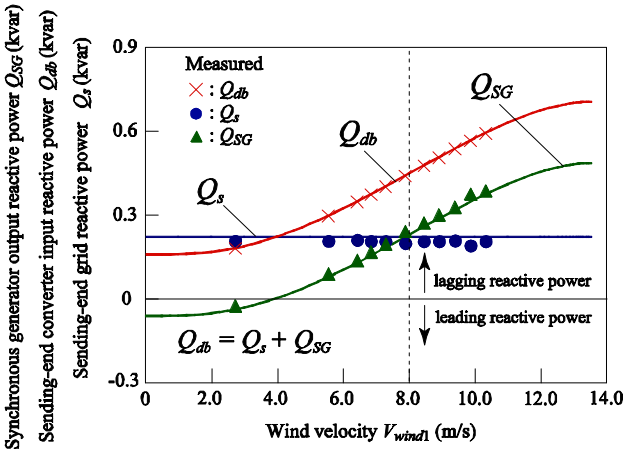

(b) Reactive power of the sending-end circuit Q_{SG}, Q_{db}, Q_s

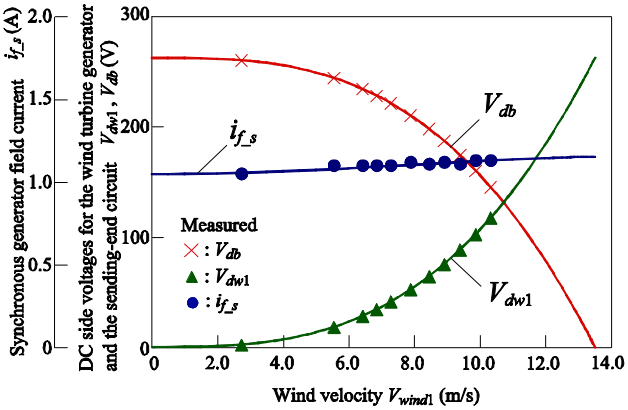

(c) Field current i_{f_s}, DC side voltages of the wind turbine generator and the sending-end circuit V_{dw1}, V_{db}

Fig. 6. Steady-state characteristics of the sending-end circuit when the wind velocity was changed

is shown that since V_{μ_s} becomes larger for the case when the power factor is leading, V_{db} becomes larger for the case of the leading power factor as shown in Fig. 7(a). Since the

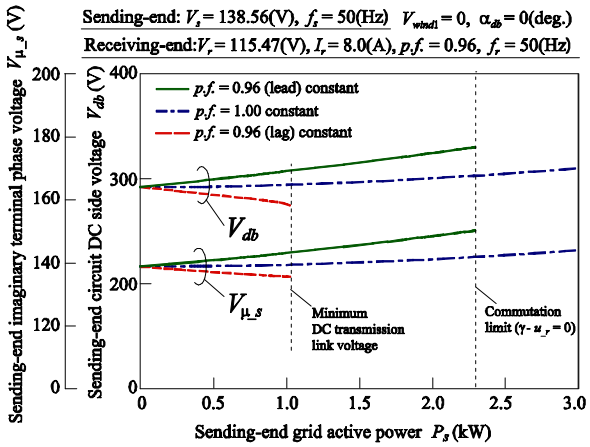

(a) Sending-end imaginary terminal phase voltage V_{μ_s} and sending-end circuit DC side voltage V_{db} vs. sending-end grid active power P_s

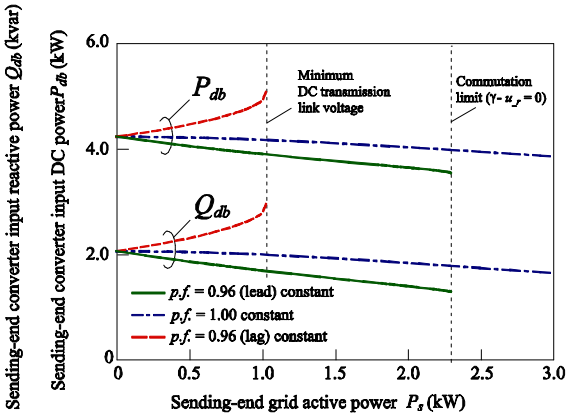

(b) Sending-end converter input active and reactive power P_{db}, Q_{db} vs. sending-end grid active power P_s

Fig. 7. Effects of the sending-end grid conditions on the system characteristics

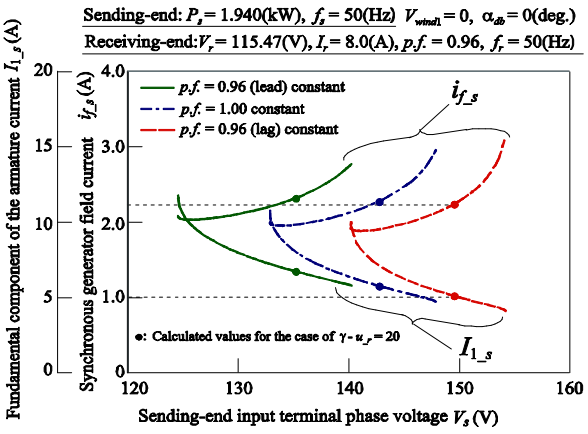

(a) Synchronous generator armature current I_{1_s} and Synchronous generator field current i_{f_s} vs. sending-end input terminal phase voltage V_s

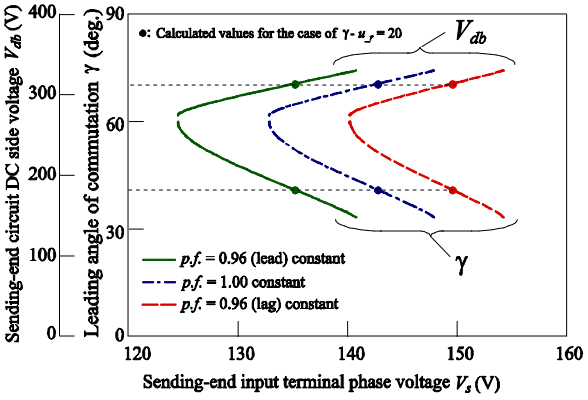

(b) Sending-end circuit DC side voltage V_{db} and leading angle of commutation for the inverter γ vs. sending-end input terminal phase voltage V_s

Fig. 8. Effects of the sending-end terminal voltage on the system characteristics

output power at the receiving-end grid should be kept constant, the increase in V_{db} causes reductions in the leading angle of commutation of the inverter γ and the DC link current I_d. Consequently, the active power and reactive power required from the converter P_{db}, Q_{db} become smaller when the sending-end grid power factor is leading. It can be seen that when the power factor is lagging, the operation limit due to the minimum DC transmission voltage may be caused by the voltage drop in L_{γ_s} and that for the case when the power factor is leading, the commutation failure for the inverter may occur due to the reduction in γ. It is also shown that the effects of the sending-end power factor are increased with the sending-end grid active power P_s.

To suppress the useless increase in the DC input power, which causes system losses, the sending-end grid power factor should be selected leading. However, in this case a large-sized synchronous generator is required because the synchronous generator provides reactive power not only for the converter but also for the sending-end grid. Furthermore, it is expected from (1) and (8) that the sending-end input terminal voltage V_s affects the DC side voltage V_{db} directly Hence, let us explore the effects of the sending-end input terminal voltage and the appropriate sending-end grid conditions for the system characteristics. Fig. 8 shows the effects of the sending-end input terminal voltage V_s on the steady-state characteristics of the system. In Fig. 8, the characteristics of the synchronous generator armature current I_{1_s}, the field current i_{f_s}, the sending-end circuit DC side voltage V_{db} and the leading angle of commutation γ versus the sending-end input terminal voltage V_s for three values of the sending-end grid power factor are shown. The marks ‘ • ’ appeared in this figure show steady-state operating points of the calculated values for the case of

$\gamma - u_{\_r}$ = 20 (deg.). The simulation conditions are given in Fig. 8(a). From Fig. 8, it is noticed that i_{f_s} and V_{db} are increased with V_s for any power factor, whereas I_{1_s} and γ are reduced with an increase in V_s. It is also shown that since V_{db} is changed in proportion to V_s as shown in Fig. 8(b), the effects of the sending-end grid power factor can be reduced by V_s. For example, as in Fig. 8(b), the same values of γ and V_{db} can be obtained by adjusting V_s even though the power factor in the sending-end grid has a different value.

As a result, when the sending-end terminal voltage V_s is selected properly, the same characteristics of the system except the sending-end circuit can be obtained even if the sending-end grid power factor is different. Consequently, the sending-end grid power factor should be selected 100% or lagging to reduce the reactive power produced by the synchronous generator, and the sending-end input terminal voltage V_s should be chosen a large value so as to reduce the effects of the sending-end grid power factor and to lessen the system losses.

4. Conclusion

In this paper, the electrical power compensation system for the DC transmission system with an integrated wind turbine generator has been proposed and its steady-state characteristics have been investigated.

The following have been concluded from the discussions:

It has been shown that a satisfactory harmonic elimination in the sending-end grid current waveform is achieved and that the sending-end grid power fluctuations due to changes in wind velocities are compensated with the proposed power compensating system.

The effects of the sending-end grid conditions on the steady-state performances for the whole system have been discussed. It has been shown that, although the reactive power required from the sending-end converter is decreased when the sending-end grid power factor is leading, the sending-end grid needs reactive power. Furthermore, since the effects of the power factor on the characteristics of the system except the sending-end circuit can be reduced by the sending-end input terminal phase voltage, the sending-end grid power factor should not be selected leading to reduce the compensation system size.

Acknowledgements

We express our sincere thanks to personnel from Gifu works, Taiyo Denki Co., Ltd. for cooperating in this study. We would also like to thank the members of NISHIKATA laboratory at Tokyo Denki University for their great assistance.

References

[1] H. Gundlach, "Static frequency converters for shaft generator systems," *The Institute of Marine Engineers*, London, UK, January 1972.

[2] S. Nishikata, A. Odaka, and Y. Koishikawa, "Steady-state performance analysis of shaft generator systems," in *Proc. Power Conversion Conference-Nagaoka*, vol. 2, pp.853-858, August 1997.

[3] S. Nishikata, K. Yamashita, F. Mita, and T. Kataoka, "A shaft generator system without output voltage distortion and its steady-state characteristics," in *Proc. 6th International Symposium on Marine Engineering*, Tokyo vol. 1, TS-28, pp. 169-174, October 2000.

[4] K. Yamashita and S. Nishikata, "Dynamic performance analysis of control systems for a shaft generator system for constant output voltage and constant frequency," *International Conference on Electrical Machines (ICEM2002)*, Brugge, Belgium, August 2002.

[5] F. Tatsuta, T. Tsuji, N. Emi, and S. Nishikata, "Studies on a wind turbine generator system using a shaft generator system," in *Proc. 8th International Conference on Electrical Machines and Systems*, Nanjing, China, pp. 931-936, September 2005.

[6] K. Yamashita and S. Nishikata, "Dynamic performance analysis of a wind turbine generator system with thyristor inverter connected to a DC transmission system," in *Proc. 9th International Conference on Electrical Machines and Systems*, Nagasaki, Japan, November 2006.

[7] K. Yamashita and S. Nishikata, "Steady-state Performance Analysis of an Integrated Wind Turbine Generating System in a DC Transmission System with Thyristor Inverter," in *Proc. 12th International Conference on Electrical Machines and Systems*, Tokyo, Japan, November 2009.

[8] S. Heier, *Grid Integration of Wind Energy Conversion Systems*, 2nd ed. New York: Wiley, 2006, p. 43.

[9] T. Kataoka and S. Nishikata, "Transient Performance Analysis of Self-Controlled Synchronous Motors," *IEEE Trans. Ind. Appl.*, vol. IA-17, No. 2, pp 152-159 (1981-3/4).

[10] IEEJ specialists committee for DC transmission, *DC Transmission Technology*, The Institute of Electrical Engineers of Japan, 1978, p. 15.

Ken-ichiro Yamashita received the D.Eng. degree in electrical engineering from Tokyo Denki University (TDU), Tokyo, Japan, in 2004. His research interests are electrical machinery and wind-turbine generator systems.

Shoji Nishikata received the B.Eng. and M.Eng. degrees from Tokyo Denki University (TDU), Tokyo, Japan, in 1972 and 1975, respectively, and the D.Eng. degree from Tokyo Institute of Technology (TIT), Tokyo, in 1984. From 1975 to 1984, he was a Research Associate at TIT. In 1984, he joined TDU, where he is currently a Professor. Dr. Nishikata is a Senior Member of IEEE, and a Senior Member of the Institute of Electrical Engineers of Japan.